

Robust M-estimation-based Tensor Ring Completion: a Half-quadratic Minimization Approach

Yicong He and George K. Atia, *Member, IEEE*,

Abstract—Tensor completion is the problem of estimating the missing values of high-order data from partially observed entries. Among several definitions of tensor rank, tensor ring rank affords the flexibility and accuracy needed to model tensors of different orders, which motivated recent efforts on tensor-ring completion. However, data corruption due to prevailing outliers poses major challenges to existing algorithms. In this paper, we develop a robust approach to tensor ring completion that uses a M-estimator as its error statistic, which can significantly alleviate the effect of outliers. Leveraging a half-quadratic (HQ) method, we reformulate the problem as one of weighted tensor completion. We present two HQ-based algorithms based on truncated singular value decomposition and matrix factorization along with their convergence and complexity analysis. Extendibility of the proposed approach to alternative definitions of tensor rank is also discussed. The experimental results demonstrate the superior performance of the proposed approach over state-of-the-art robust algorithms for tensor completion.

Index Terms—M-estimator, robust method, tensor completion, half-quadratic.

1 INTRODUCTION

Predicting missing information from partially observed data is an emerging topic in modern data science due to an unprecedented growth in data volume and dimensionality [1]. In multi-way data analysis where the data can be represented as a high-order tensor, this problem can be formulated in the lens of tensor completion with the goal of recovering the missing entries of a partially observed tensor. While the tensor completion problem is ill-posed without further model assumptions, actual formulations exploit the low rank structures intrinsic to much of the data. Numerous tensor completion algorithms have been proposed based on different definitions of the tensor rank, such as CP rank [2], Tucker rank [3], [4], [5], [6], tubal rank [7], [8], [9], tensor ring [10], [11], [12], [13] and tensor train rank-based algorithms [14], [15].

Among existing tensor rank models, tensor ring (TR) rank has shown desirable performance in many tensor completion tasks owing to its flexibility [16]. TR rank is established from TR decomposition in which a high-order tensor is factorized into a sequence of circularly contracted 3-order core tensors [10], [17]. Several algorithms that directly find the core tensors have been developed, such as tensor ring weighted optimization (TR-WOPT) [16] and hierarchical tensor ring completion [18]. To further improve efficiency, an efficient circular TR unfolding scheme was proposed in [12], [13], which was leveraged by some algorithms, including tensor ring nuclear norm minimization (TRNNM) [19] and parallel matrix factorization [13].

Real-world data may be corrupted by outliers due to human error or signal interference, making some of the observed data unreliable. Since the aforementioned tensor-ring-based completion algorithms are based on a second-order measure of the error residuals, their performance degrades in presence of outliers. In order to enhance robustness, a common practice in machine learning has been to use more robust norms such as the l_1 -norm. For example, [20] proposes a robust tensor ring completion algorithm where the Frobenius norm of TRNNM is replaced with the robust l_1 -norm. However, the non-smoothness and non-differentiability of the l_1 -norm at zero often lead to loss in accuracy and computational efficiency.

In this paper, we develop an optimization framework for robust tensor completion wherein a M-estimator is introduced for the error statistic to improve robustness. M-estimators rooted in robust statistics are generalizations of maximum likelihood (ML) estimators for which the objective function is a sample average [21]. The selection of a proper loss function for M-estimators can greatly enhance robustness against large outliers. In order to handle the complex objective resulting from the use of a M-estimator, we leverage a half-quadratic (HQ) [22] minimization approach whereby the problem is reformulated as a weighted tensor completion program.

By introducing a tensor ring model in the proposed completion framework, we propose a novel cost function for the robust tensor ring completion problem. Based on a TR unfolding scheme, we develop two robust tensor ring completion algorithms, which utilize truncated singular value decomposition (SVD) and matrix factorization to capture the low rank structure. Benefiting from a HQ-based method and a TR unfolding scheme, the proposed robust algorithms are efficient and have a simple structure. Further, the convergence and complexity of the proposed algorithms

• Yicong He and George K. Atia are with the Department of Electrical and Computer Engineering, University of Central Florida, Orlando, FL, 32816, USA.
E-mails: Yicong.He@ucf.edu, George.Atia@ucf.edu.

are analyzed.

We also discuss the relation of the proposed algorithms to existing tensor ring completion methods, showing that earlier methods can be viewed as special cases of the robust algorithms proposed. We also show that the proposed robust completion framework can be easily applied to other tensor rank models. For example, it can be used to obtain robust versions of existing l_2 -based tensor completion algorithms. The following summarizes the main contributions of the paper.

- 1) We propose a unified solution for robust tensor completion by introducing a M-estimator as the error statistic, and leveraging a HQ method to transform the complex optimization problem to a weighted tensor completion problem.
- 2) Based on a TR unfolding scheme, we develop two robust tensor ring completion algorithms, which utilize truncated SVD and matrix factorization to capture the low rank structure, and present their convergence and complexity analysis.
- 3) We perform experiments on real data for image inpainting and denoising, and video completion, demonstrating the superior performance of the proposed algorithms compared with existing tensor ring completion and other robust tensor completion algorithms.

The paper is organized as follows. In Section 2 we introduce our M-estimation-based robust tensor completion framework using the HQ method. In Section 3, we propose two new HQ-based tensor ring completion based on truncated SVD and matrix factorization. We also discuss connections to current algorithms and extensions to other rank models. In Section 4, the convergence analysis of the proposed algorithms is presented. Experimental results are presented in Section 5 to demonstrate the reconstruction performance. Finally, the conclusion is given in Section 6.

Notation: Uppercase script letters are used to denote tensors (e.g., \mathcal{X}), and boldface letters to denote matrices (e.g., \mathbf{X}). A N -order tensor is defined as $\mathcal{X} \in \mathbb{R}^{I_1 \times \dots \times I_N}$, where $I_i, i = 1, \dots, N$, is the dimension of the i -th way of the tensor. $\mathcal{X}_{i_1 \dots i_N}$ denotes the (i_1, i_2, \dots, i_N) -th entry of tensor \mathcal{X} , and $\mathbf{X}_{i,j}$ the (i, j) -th entry of matrix \mathbf{X} . The Frobenius norm of a tensor is defined as $\|\mathcal{X}\|_F = \sqrt{\sum_{i_1 \dots i_N} |\mathcal{X}_{i_1 \dots i_N}|^2}$. The product $\mathcal{A} \circ \mathcal{B}$ denotes the Hadamard (element-wise) product of tensors \mathcal{A} and \mathcal{B} .

2 HALF-QUADRATIC FRAMEWORK FOR M-ESTIMATOR-BASED TENSOR COMPLETION

We formulate robust tensor completion as a M-estimator-based optimization problem, and propose a HQ method as a solution. In this section, we keep the definition of tensor rank general for potential extendibility of the solution. Specialization to TR rank is considered in Section 3.

2.1 Generalization of tensor completion

Given a N -order tensor $\mathcal{M} \in \mathbb{R}^{I_1 \times \dots \times I_N}$, and index set $\Omega \subseteq [I_1] \times \dots \times [I_N]$, tensor completion is the problem of filling in the missing entries of tensor \mathcal{M} using the observed

entries indexed by set Ω and the low rank property. This problem can be formulated as

$$\min_{\mathcal{X}} \text{rank}_t(\mathcal{X}), \text{ s.t. } \mathcal{P} \circ \mathcal{X} = \mathcal{P} \circ \mathcal{M} \quad (1)$$

where the mask tensor $\mathcal{P} \in \mathbb{R}^{I_1 \times \dots \times I_N}$ is set as

$$\mathcal{P}_{i_1 \dots i_N} = \begin{cases} 1, & \text{if } (i_1, \dots, i_N) \in \Omega \\ 0, & \text{otherwise} \end{cases} \quad (2)$$

$\text{rank}_t(\mathcal{X})$ denotes the rank of tensor \mathcal{X} , which varies depending on different definitions of tensor rank. Alternatively, one can use the unconstrained form

$$\min_{\mathcal{X}} \text{rank}_t(\mathcal{X}) + \lambda \|\mathcal{P} \circ (\mathcal{X} - \mathcal{M})\|_F^2, \quad (3)$$

where λ is the regularization parameter. Since solving (1) or (3) is NP-hard, it is common to replace the rank term with a tractable surrogate (e.g., the nuclear norm). Thus, one can further generalize the tensor completion task to solving

$$\min_{\mathcal{X}} \Phi(\mathcal{X}) + \lambda \|\mathcal{P} \circ (\mathcal{X} - \mathcal{M})\|_F^2, \quad (4)$$

where $\Phi(\mathcal{X})$ is a general rank constraint on tensor \mathcal{X} .

2.2 M-estimator-based robust tensor completion

In robust statistics, the M-estimator has been widely used due to its robustness to outliers. For a tensor \mathcal{X} , its M-estimator $F(\mathcal{X})$ can be formed as a sum of functions of the data, i.e., $F(\mathcal{X}) = \sum_{i_1 \dots i_N} f(\mathcal{X}_{i_1 \dots i_N})$, where $f(\cdot)$ is a function with certain properties. By introducing the M-estimator in (4), we obtain the M-estimator-based robust tensor completion optimization problem

$$\min_{\mathcal{X}} \Phi(\mathcal{X}) + \lambda F_{\Omega}(\mathcal{X} - \mathcal{M}), \quad (5)$$

where $F_{\Omega}(\mathcal{X}) = \sum_{i_1 \dots i_N \in \Omega} f(\mathcal{X}_{i_1 \dots i_N})$.

In our work, we use three functions for M-estimators: Huber function, Welsch (correntropy) function [23], [24] and Cauchy function shown in Fig.1. The Welsch and Cauchy functions yield a type of redescending M-estimators, which also satisfy that $\lim_{t \rightarrow +\infty} f'(t) = 0$. In [5], a redescending M-estimator is introduced for low-Tucker-rank tensor completion, and the solution is obtained using a block coordinate descent method. In the next subsection, we exploit the properties of M-estimators to develop a more general and simpler algorithm for robust tensor completion.

2.3 Half-quadratic-based robust tensor completion

We present a half-quadratic method to solve the M-estimator-based optimization problem in (5). Half-quadratic (HQ) methods have been applied in non-quadratic optimization [25]. Rather than directly optimizing a complex non-quadratic problem, HQ transforms the non-quadratic loss function to a half-quadratic one. Specifically, there exists a strictly convex and decreasing dual function [25], [26] $\varphi(\cdot)$ such that minimizing the loss function $f(t)$ with respect to (w.r.t.) t is equivalent to minimizing an augmented cost function in an enlarged parameter space $\{t, w\}$, i.e.,

$$\min_t f(t) = \min_{t, w} \frac{1}{2} wt^2 + \varphi(w). \quad (6)$$

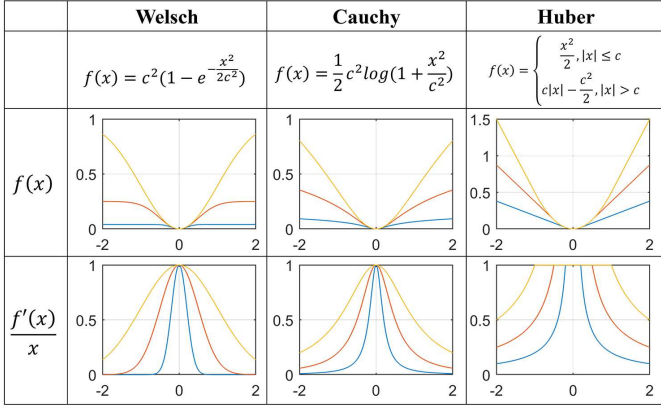


Fig. 1. Illustration of loss functions (top) and corresponding weight function (bottom) with different parameter c (Blue: $c = 0.2$, red: $c = 0.5$, yellow: $c = 1$).

Therefore, by substituting (6) in the definition of F_Ω , the minimization of function $F_\Omega(\mathcal{X} - \mathcal{M})$ becomes

$$\min_{\mathcal{X}} F_\Omega(\mathcal{X} - \mathcal{M}) = \min_{\mathcal{X}, \mathcal{W}} \sum_{i_1 \dots i_N \in \Omega} \frac{1}{2} \mathcal{W}_{i_1 \dots i_N} \mathcal{E}_{i_1 \dots i_N}^2 + \varphi(\mathcal{W}_{i_1 \dots i_N}) \quad (7)$$

where $\mathcal{E}_{i_1 \dots i_N} = \mathcal{X}_{i_1 \dots i_N} - \mathcal{M}_{i_1 \dots i_N}$ is the error residual tensor. Hence, (5) can be transformed to the minimization

$$\min_{\mathcal{X}, \mathcal{W}} \Phi(\mathcal{X}) + \frac{\lambda}{2} \|\sqrt{\mathcal{W}} \circ \mathcal{P} \circ (\mathcal{X} - \mathcal{M})\|_F^2 + \lambda \Psi_\Omega(\mathcal{W}) \quad (8)$$

where $\Psi_\Omega(\mathcal{W}) = \sum_{i_1 \dots i_N \in \Omega} \varphi(\mathcal{W}_{i_1 \dots i_N})$.

One could use alternating minimization to solve (8). Specifically, by fixing tensor \mathcal{X} , tensor \mathcal{W} can be found by solving (8) with fixed residual \mathcal{E} . According to Theorem 1 in [26], the optimal solution \hat{w} in the RHS of (6) can be obtained as $\hat{w} = \frac{f'(t)}{t}$. Thus, we obtain $\mathcal{W}_{i_1 \dots i_N}, (i_1 \dots i_N) \in \Omega$ as

$$\mathcal{W}_{i_1 \dots i_N} = \frac{f'(\mathcal{E}_{i_1 \dots i_N})}{\mathcal{E}_{i_1 \dots i_N}}. \quad (9)$$

Subsequently, given a fixed \mathcal{W} , (8) becomes the weighted tensor completion problem

$$\min_{\mathcal{X}} \Phi(\mathcal{X}) + \frac{\lambda}{2} \|\sqrt{\mathcal{W}} \circ \mathcal{P} \circ (\mathcal{X} - \mathcal{M})\|_F^2. \quad (10)$$

The weighting tensor \mathcal{W} assigns different weights to each observed entry based on the error residual tensor \mathcal{E} . Fig. 1 depicts the weights in terms of the error (x) for different loss functions. One can observe that a large error leads to a small weight, so that the error statistics are not unduly affected by large outliers.

2.4 Adaptive parameter selection for M-estimator

Most M-estimators such as Huber, Cauchy and Welsch have a parameter c to control the shape of the loss. Per the previous discussion, the weights \mathcal{W} based on the error residual play an important role in recognizing the outliers. Weights \mathcal{W} for different values of the shape parameter c are depicted in Fig.1 (bottom). In this paper, we use an adaptive kernel width selection method for the M-estimator. Specifically, the shape parameter is determined by

$$c = \max(\eta(\max(\mathbf{e}_\Omega(0.25), \mathbf{e}_\Omega(0.75))), c_{\min}) \quad (11)$$

where $\mathbf{e}_\Omega \in \mathbb{R}^{|\Omega| \times 1}$ denotes the vector composed of entries $\mathcal{E}_{i_1 \dots i_N}, i_1 \dots i_N \in \Omega$, and $\mathbf{y}_{(q)}$ denotes the q -th quantile of \mathbf{y} . The parameter η controls the range of outliers, and c_{\min} is a lower bound on c .

3 HQ-BASED ROBUST TENSOR RING COMPLETION

In this section, we use the tensor ring as the tensor rank model and develop two efficient algorithms to our formulation based on truncated SVD and matrix factorization. We also comment on extendibility to other rank models.

3.1 TR decomposition and TR unfolding

First, we briefly review the definition of TR decomposition.

Definition 1 (TR Decomposition [17]). *Given TR rank $[r_1, \dots, r_N]$, in TR decomposition a high-order tensor $\mathcal{X} \in \mathbb{R}^{I_1 \times \dots \times I_N}$ is represented as a sequence of circularly contracted 3-order core tensors $\mathcal{U}_k \in \mathbb{R}^{r_k \times I_k \times r_{k+1}}, k = 1, \dots, N$, with $r_{N+1} = r_1$. Specifically, the element-wise relation of tensor \mathcal{X} and its TR core tensors $\{\mathcal{U}_k\}_{k=1}^N$ is defined as*

$$\mathcal{X}_{i_1 \dots i_N} = \text{Tr} \left(\prod_{k=1}^N \mathcal{U}_k(:, k, :) \right),$$

where $\mathcal{U}_k(:, k, :) \in \mathbb{R}^{r_k \times r_{k+1}}$ is the slice matrix of \mathcal{U}_k along mode-2, and $\text{Tr}(\cdot)$ is the matrix trace operator.

Given the above definition and the low TR rank assumption, [16] and [18] solve the tensor ring completion problem by directly finding the core tensors $\{\mathcal{U}_k\}_{k=1}^N$. Therefore, these completion algorithms generally suffer from high computational complexity. The authors in [12], [13] proposed a new circular TR unfolding scheme. In particular, the TR unfolding is defined as follows.

Definition 2 (TR unfolding [12], [19]). *Given an N -order tensor $\mathcal{X} \in \mathbb{R}^{I_1 \times \dots \times I_N}$, its TR unfolding $\mathbf{X}_{\langle k, d \rangle} \in \mathbb{R}^{\prod_{i=k}^{k+d-1} I_i \times \prod_{j=k+d}^{k+N-1} I_j}$ is a matrix whose entries are defined through the relation $(\mathbf{X}_{\langle k, d \rangle})_{s, t} = \mathcal{X}_{i_1 \dots i_N}$ with*

$$s = 1 + \sum_{c=k}^{k+d-1} (i_c - 1) \prod_{j=k}^{c-1} I_j, \quad t = 1 + \sum_{c=k+d}^{k+N-1} (i_c - 1) \prod_{j=k+d}^{c-1} I_j$$

where $I_{k+N} = I_k, i_{k+N} = i_k$ for $k = 1, \dots, N$. In practice, $\mathbf{X}_{\langle k, d \rangle}$ can be generated by first permuting \mathcal{X} with order $[k, \dots, N, 1, \dots, k-1]$, then performing unfolding along the first d modes.

If the unfoldings of \mathcal{X} follow Definition 2, the rank of $\mathbf{X}_{\langle k, d \rangle}$ obeys the inequality $\text{rank}(\mathbf{X}_{\langle k, d \rangle}) \leq r_k r_{k+d}$ with $r_{i+N} = r_i, i = 1, \dots, N$ [12], [19]. Thus, the M-estimator-based robust tensor ring completion problem can be formulated as

$$\min_{\mathcal{X}} F_\Omega(\mathcal{X} - \mathcal{M}), \text{ s.t. } \text{rank}(\mathbf{X}_{\langle k, d \rangle}) \leq \hat{r}_k, k = 1, \dots, N \quad (12)$$

where \hat{r}_k is the estimated upper bound on the rank of matrix $\mathbf{X}_{\langle k, d \rangle}$. The formulation in (12) cannot be directly solved using the HQ method in its current form. In the following, we reformulate (12) in two different unconstrained forms and propose two different approaches to their solution.

3.2 Truncated SVD-based algorithm

The first method is based on low rank approximation. Defining the indicator function for $\mathbf{X}_{\langle k, d \rangle}$, $k = 1, \dots, N$ as

$$\delta(\mathbf{X}_{\langle k, d \rangle}) = \begin{cases} 0, & \text{if } \text{rank}(\mathbf{X}_{\langle k, d \rangle}) \leq r_k \\ +\infty, & \text{otherwise} \end{cases}, \quad (13)$$

(12) can be reformulated as (5) with $\Phi(\mathcal{X}) = \sum_{k=1}^N \beta_k \delta(\mathbf{X}_{\langle k, d \rangle})$, where $\{\beta_k\}_{k=1}^N$ are weight parameters. Thus, the minimization is expressed as

$$\min_{\mathcal{X}, \mathcal{W}} \sum_{k=1}^N \beta_k \delta(\mathbf{X}_{\langle k, d \rangle}) + \frac{\lambda}{2} \|\sqrt{\mathcal{W}} \circ \mathcal{P} \circ (\mathcal{M} - \mathcal{X})\|_F^2 + \lambda \Psi_{\Omega}(\mathcal{W}) \quad (14)$$

We use an ADMM method to solve (14). In particular, we introduce the dual variables $\{\mathcal{Z}^{(k)}\}_{k=1}^N$ and rewrite (14) as

$$\min_{\mathcal{X}, \mathcal{W}, \mathcal{Z}^{(k)}} \sum_{k=1}^N \beta_k \delta(\mathbf{Z}_{\langle k, d \rangle}^{(k)}) + \frac{\lambda}{2} \|\sqrt{\mathcal{W}} \circ \mathcal{P} \circ (\mathcal{M} - \mathcal{X})\|_F^2 + \lambda \Psi_{\Omega}(\mathcal{W}) \quad \text{s.t. } \mathcal{Z}^{(k)} = \mathcal{X}, \quad k=1, \dots, N \quad (15)$$

The augmented Lagrangian function can be written as

$$\begin{aligned} \mathcal{L}(\mathcal{X}, \mathcal{W}, \mathcal{Z}^{(1)}, \dots, \mathcal{Z}^{(N)}, \mathcal{G}^{(1)}, \dots, \mathcal{G}^{(N)}) \\ = \sum_{k=1}^N \left(\beta_k \delta(\mathbf{Z}_{\langle k, d \rangle}^{(k)}) + \langle \mathcal{G}^{(k)}, \mathcal{Z}^{(k)} - \mathcal{X} \rangle + \frac{\mu}{2} \|\mathcal{Z}^{(k)} - \mathcal{X}\|_F^2 \right) \\ + \frac{\lambda}{2} \|\sqrt{\mathcal{W}} \circ \mathcal{P} \circ (\mathcal{M} - \mathcal{X})\|_F^2 + \lambda \Psi_{\Omega}(\mathcal{W}) \end{aligned} \quad (16)$$

where \mathcal{G} are the dual variables and μ is the step size. One can alternatively update each variable while fixing the others:

1) Update c and \mathcal{W} : First, c is estimated using (11). Then, for each element $\mathcal{W}_{i_1 \dots i_N, i_1 \dots i_N} \in \Omega$, the optimal solution can be directly obtained using (9).

2) Update $\mathcal{Z}^{(k)}$: For each $\mathcal{Z}^{(k)}$, $k = 1, \dots, N$, the optimal solution can be obtained by

$$\mathcal{Z}^{(k)} = \arg \min_{\mathcal{Z}} \|\mathcal{Z} - (\mathcal{X} - \frac{1}{\mu} \mathcal{G}^{(k)})\|_F^2 \quad \text{s.t. } \text{rank}(\mathbf{Z}_{\langle k, d \rangle}) \leq \hat{r}_k \quad (17)$$

This is a low rank approximation problem which has optimal solution [27]

$$\mathcal{Z}^{(k)} = \text{fold}_{\langle k, d \rangle} \left(\Pi_{\hat{r}_k}(\mathbf{X}_{\langle k, d \rangle}) - \frac{1}{\mu} \mathbf{G}_{\langle k, d \rangle}^{(k)} \right), \quad (18)$$

where $\Pi_r(\cdot)$ is the truncated SVD (or hard thresholding) operator with rank r , and $\text{fold}_{\langle k, d \rangle}(\cdot)$ is the reverse operation of TR unfolding.

3) Update \mathcal{X} : Tensor \mathcal{X} can be obtained as

$$\begin{aligned} \mathcal{X} = \arg \min_{\mathcal{X}} \frac{\lambda}{\mu} \|\sqrt{\mathcal{W}} \circ \mathcal{P} \circ (\mathcal{M} - \mathcal{X})\|_F^2 \\ + \sum_{k=1}^N \|\mathcal{X} - (\mathcal{Z}^{(k)} + \frac{1}{\mu} \mathcal{G}^{(k)})\|_F^2. \end{aligned} \quad (19)$$

By taking the derivative of \mathcal{X} and setting it to be the zero tensor, we obtain the optimal solution

$$\mathcal{X} = \mathcal{Q} + \frac{\lambda \mathcal{W}}{\lambda \mathcal{W} + \mu N} \circ \mathcal{P} \circ (\mathcal{M} - \mathcal{Q}), \quad (20)$$

where $\mathcal{Q} = \frac{1}{N} \sum_{k=1}^N (\mathcal{Z}^{(k)} + \frac{1}{\mu} \mathcal{G}^{(k)})$.

4) Update $\mathcal{G}^{(k)}$: For each k , $\mathcal{G}^{(k)}$ can be updated as

$$\mathcal{G}^{(k)} = \mathcal{G}^{(k)} + \mu (\mathcal{Z}^{(k)} - \mathcal{X}). \quad (21)$$

We name this algorithm Half-Quadratic Tensor Ring Completion by Truncated SVD (HQTRC-TS). The pseudocode for HQTRC-TS is summarized in Algorithm 1.

Algorithm 1 HQTRC-TS for robust tensor completion

Input: $\mathcal{P}, \mathcal{P} \circ \mathcal{M}, d, \mu, \alpha, \{\hat{r}_k\}_{k=1}^N, \lambda$ and ϵ
 1: initial tensors $\{\mathcal{G}^{(k),0}\}_{k=1}^N = \mathbf{0}, \mathcal{X}^0 = \mathcal{X}^1 = \mathbf{0}, t = 1$
 2: **repeat**
 3: estimate c^{t+1} using (11).
 4: compute \mathcal{W}^{t+1} using (9).
 5: compute $\mathcal{Z}^{(k),t+1}$ for $k = 1, \dots, N$ using (17).
 6: compute \mathcal{X}^{t+1} using (20).
 7: compute $\mathcal{G}^{(k),t+1}$ for $k = 1, \dots, N$ using (21).
 8: update $\mu^{t+1} = \alpha \mu^t$
 9: $t = t + 1$
 10: **until** $\|\mathcal{X}^{t-1} - \mathcal{X}^{t-2}\|_F / \|\mathcal{X}^{t-2}\|_F - \|\mathcal{X}^t - \mathcal{X}^{t-1}\|_F / \|\mathcal{X}^{t-1}\|_F < \epsilon$
Output: \mathcal{X}^t

3.3 Matrix factorization-based algorithm

Although HQTRC-TS applies truncated SVD which can save computations compared with the full SVD, it can still be time consuming when dealing with large scale data. On the other hand, the low rank constraint can be satisfied using a matrix factorization method [13]. Therefore, we recast the problem by formulating a matrix factorization-based objective function. For each k , the matrix $\mathbf{X}_{\langle k, d \rangle}$ is factorized into the product of two small matrices $\mathbf{U}_k \in \mathbb{R}^{\prod_{i=k}^{k+d-1} I_i \times \hat{r}_k}$ and $\mathbf{V}_k \in \mathbb{R}^{\hat{r}_k \times \prod_{j=k+d}^{k-1} I_j}$. Thus, the objective function can be formulated as

$$\begin{aligned} \min_{\mathcal{X}, \mathbf{U}_k, \mathbf{V}_k, \mathcal{W}} \sum_{k=1}^N \frac{\beta_k}{2} \|\mathbf{U}_k \mathbf{V}_k - \mathbf{X}_{\langle k, d \rangle}\|_F^2 \\ + \frac{\lambda}{2} \|\sqrt{\mathcal{W}} \circ \mathcal{P} \circ (\mathcal{M} - \mathcal{X})\|_F^2 + \lambda \Psi_{\Omega}(\mathcal{W}) \end{aligned} \quad (22)$$

The optimization problem above can be efficiently solved via block coordinate descent (BCD). The variables are updated as follows:

- 1) Update c and \mathcal{W} using (11) and (9), respectively.
- 2) Update \mathcal{X} : \mathcal{X} is obtained in a similar manner as (20)

$$\begin{aligned} \mathcal{X} = \arg \min_{\mathcal{X}} \sum_{k=1}^N \beta_k \|\mathbf{U}_k \mathbf{V}_k - \mathbf{X}_{\langle k, d \rangle}\|_F^2 \\ + \lambda \|\sqrt{\mathcal{W}} \circ \mathcal{P} \circ (\mathcal{M} - \mathcal{X})\|_F^2 \quad (23) \\ = \mathcal{L} + \frac{\lambda \mathcal{W}}{\lambda \mathcal{W} + \sum_{k=1}^N \beta_k} \circ \mathcal{P} \circ (\mathcal{M} - \mathcal{L}) \end{aligned}$$

where $\mathcal{L} = \frac{1}{\sum_{k=1}^N \beta_k} \sum_{k=1}^N \beta_k \text{fold}_{\langle k, d \rangle}(\mathbf{U}_k \mathbf{V}_k)$.

3) Update \mathbf{U}_k and \mathbf{V}_k : For each k , we obtain \mathbf{U}_k and \mathbf{V}_k as

$$\mathbf{U}_k = \mathbf{X}_{\langle k, d \rangle} \mathbf{V}_k^T (\mathbf{V}_k \mathbf{V}_k^T)^{-1} \quad (24)$$

$$\mathbf{V}_k = (\mathbf{U}_k^T \mathbf{U}_k)^{-1} \mathbf{U}_k^T \mathbf{X}_{\langle k, d \rangle} \quad (25)$$

We name the above algorithm Half-Quadratic Tensor Ring Completion by Matrix Factorization (HQTRC-MF). The pseudocode for HQTRC-MF is presented in Algorithm 2.

Algorithm 2 HQTRC-MF for robust tensor completion

Input: $\mathcal{P}, \mathcal{P} \circ \mathcal{M}, d, \beta, \{\hat{r}_k\}_{k=1}^N, \lambda$ and ϵ
 1: initial matrices \mathbf{U}_k^0 and $\mathbf{V}_k^0, t = 0$
 2: **repeat**
 3: estimate c^{t+1} using (11).
 4: compute \mathcal{W}^{t+1} using (9).
 5: compute \mathcal{X}^{t+1} using (23).
 6: compute \mathbf{U}_k^{t+1} for $k = 1, \dots, N$ using (24).
 7: compute \mathbf{V}_k^{t+1} for $k = 1, \dots, N$ using (25).
 8: $t = t + 1$
 9: **until** $\|\mathcal{X}^t - \mathcal{X}^{t-1}\|_F / \|\mathcal{X}^{t-1}\|_F < \epsilon$
Output: \mathcal{X}^t

3.4 Relation to prior tensor completion algorithms

To better understand the relationship between the proposed algorithms and existing l_2 norm-based tensor ring completion algorithms, we first rewrite (23) element-wise as

$$\begin{aligned} \mathcal{X}_{i_1 \dots i_N} &= \begin{cases} \Theta_{i_1 \dots i_N} \mathcal{M}_{i_1 \dots i_N} + (1 - \Theta_{i_1 \dots i_N}) \mathcal{L}_{i_1 \dots i_N}, & i_1 \dots i_N \in \Omega \\ \mathcal{L}_{i_1 \dots i_N}, & i_1 \dots i_N \notin \Omega \end{cases} \end{aligned} \quad (26)$$

with $\Theta = \frac{\lambda \mathcal{W}}{\lambda \mathcal{W} + \sum_{k=1}^N \beta_k}$, where division and addition are element-wise. Eq. (20) can be rewritten in the same manner by setting $\Theta = \frac{\lambda \mathcal{W}}{\lambda \mathcal{W} + \mu N}$. When using the Frobenius norm as the error measure, all the entries of \mathcal{W} are 1 and the cost function in (8) reduces to (4). Further, when the regularization parameter λ is sufficiently large, all entries $\Theta_{i_1 \dots i_N}$ will be 1 and (26) reduces to

$$\mathcal{X} = \begin{cases} \mathcal{M}_{i_1 \dots i_N}, & i_1 \dots i_N \in \Omega \\ \mathcal{L}_{i_1 \dots i_N}, & i_1 \dots i_N \notin \Omega \end{cases} \quad (27)$$

in which case Algorithm 2 reduces to PTRC [13]. The update of \mathcal{X} for HQTRC-TS with $\lambda \rightarrow \infty$ can also be simplified to the form (27) by just replacing \mathcal{L} with \mathcal{Q} from Eq.(20), in which case Algorithm 1 reduces to a modified version of TRNNM (TRNNM uses singular value thresholding (SVT) rather than truncated SVD). Thus, these earlier algorithms for tensor ring completion are special cases of the two proposed algorithms.

When the regularization parameter λ is properly chosen, the elements of \mathcal{W} will assign different weights to different values of the error residuals. It can be observed from Fig.1 that a large error residual $\mathcal{E}_{i_1 \dots i_N}$ caused by an outlier may result in a small $\mathcal{W}_{i_1 \dots i_N}$ (consequently a small $\Theta_{i_1 \dots i_N}$). In this case, the values of the entries with large error residuals will be dominated by the predicted value \mathcal{Q} rather than \mathcal{M} . If the error residual is large enough, θ will be zero so the corresponding entry will be set to the corresponding entry in \mathcal{Q} , which amounts to treating it as a missing entry. In general, by assigning different weights to observed entries, the proposed algorithms can automatically identify the outliers.

3.5 Extension to other tensor models

The robust approach proposed to tensor completion can be extended to other tensor rank models by replacing $\Phi(\mathcal{X})$ in (8) with a new constraint that depends on the rank model.

In order to illustrate the idea, we will use the tubal rank (i.e., t-SVD) as an example. In t-SVD-based tensor completion [7], [28], minimizing the tubal rank of a tensor $\mathcal{X} \in \mathbb{R}^{n_1 \times n_2 \times n_3}$ is approximated by the minimization of the tensor nuclear norm (TNN)

$$\|\mathcal{X}\|_* = \frac{1}{n_3} \sum_{i=1}^{n_3} \|\bar{\mathbf{X}}^{(i)}\|_* \quad (28)$$

where $\bar{\mathbf{X}}^{(i)}$ is the i -th frontal slice of tensor $\bar{\mathcal{X}}$, and $\bar{\mathcal{X}} = \text{fft}(\mathcal{X}, [1, 3])$ denotes the Fourier transform of \mathcal{X} along the third dimension.

Therefore, by replacing $\Phi(\mathcal{X})$ in (8) with the TNN defined in (28), one can obtain a cost function for a M-estimation-based t-SVD completion algorithm – we name it HQTNN as an extension of TNN. Specifically, the HQTNN algorithm can be directly derived with a similar form to HQTRC-TS by setting $N = 1$ and replacing (17) in step 5 of Algorithm 1 with the following TNN-based optimization problem

$$\mathcal{Z} = \arg \min_{\mathcal{Z}} \frac{1}{2} \|\mathcal{Z} - (\mathcal{X} - \frac{1}{\mu} \mathcal{G})\|_F^2 + \|\mathcal{Z}\|_* \quad (29)$$

We remark that, similar to (18), (29) also has a closed-form solution. The reader is referred to [7] for more details.

Apart from the t-SVD-based tensor model, the proposed framework can also be applied to other rank models such as Tucker and CP rank. Further, by setting the tensor order to 2, the proposed algorithm can also be applied to robust matrix completion. The foregoing outlier identification capability will be inherited by robust algorithms developed for different tensor/matrix rank models.

3.6 Complexity analysis

Let $r_{\max} = \max\{\hat{r}_k\}_{k=1}^N$ and $I_{\max} = \max\{I_k\}_{k=1}^N$. For HQTRC-TS, computing \mathcal{W}, \mathcal{X} and $\mathcal{G}^{(k)}$ for each k has complexity $\mathcal{O}(I_{\max}^N)$. For $\mathcal{Z}^{(k)}$, the computational cost of solving the truncated SVD problem is $\mathcal{O}(I_{\max}^N r_{\max}^2)$. Therefore, the total cost of HQTRC-TS is $\mathcal{O}(N I_{\max}^N r_{\max}^2)$.

For HQTRC-MF, computing \mathcal{W} and \mathcal{X} incurs complexity $\mathcal{O}(I_{\max}^N)$. For each k , computing \mathbf{U}_k and \mathbf{V}_k has complexity $\mathcal{O}(I_{\max}^N r_{\max}^2 + r_{\max}^6)$, i.e., $\mathcal{O}(I_{\max}^N r_{\max}^2)$ since $r_{\max}^2 \leq \min\{I_{\max}^d, I_{\max}^{N-d}\}$. Therefore, the order complexity of HQTRC-MF is $\mathcal{O}(N I_{\max}^N r_{\max}^2)$, similar to HQTRC-TS. However, in practice HQTRC-MF has much smaller running time than HQTRC-TS since solving the truncated SVD requires a number of iterations.

4 CONVERGENCE ANALYSIS

The following theorems characterize the convergence of the proposed algorithms. For simplicity, we define $\mathbf{U}_a = \{\mathbf{U}_k\}_{k=1}^N$, $\mathbf{V}_a = \{\mathbf{V}_k\}_{k=1}^N$, $\mathcal{Z}_a = \{\mathcal{Z}^{(k)}\}_{k=1}^N$ and $\mathcal{G}_a = \{\mathcal{G}^{(k)}\}_{k=1}^N$.

Theorem 1 (HQTRC-TS convergence). *Let $\{\mathcal{X}^t, \mathcal{W}^t, \mathcal{Z}_a^t, \mathcal{G}_a^t\}$ be a sequence generated by Algorithm 1 using the loss functions*

defined in Fig. 1. If the sequence $\{\mathcal{G}^{(k),t}\}$ converges to some constant tensor \mathcal{C} for all $k = 1, \dots, N$, then $\{\mathcal{X}^t\}$ will converge for a M-estimator parameter c decreasing to 0.

Theorem 2 (HQTRC-MF convergence). *Let $\{\mathcal{X}^t, \mathcal{W}^t, \mathbf{U}_a^t, \mathbf{V}_a^t\}$ be a sequence generated by Algorithm 2 using the loss functions defined in Fig. 1. Then, for a M-estimator parameter c decreasing to 0, the sequence $\{\mathcal{X}^t\}$ will converge.*

The proof are deferred to Appendix A and C, respectively. In these theorems, a sequence $\{c^t\}$ with $\lim_{t \rightarrow \infty} c^t = 0$ is sufficient to ensure convergence of both HQTRC-TS and HQTRC-MF. In practice, adaptive parameter selection using (11) yields a sequence $\{c^t\}$ that approaches a small c_{min} , albeit not monotonically decreasing. Still, it yields desirable performance as shown in the experimental results.

Since HQTRC-TS is a non-convex optimization problem due to the use of a truncated SVD, the convergence analysis of ADMM is very challenging in general without additional assumptions [29]. Hence, similar to [30], [31], [32], the assumption of the convergence of $\{\mathcal{G}^{(k),t}\}$ is used in Theorem 1. In practice, HQTRC-TS using Algorithm 1 works very well, which is verified in Section 5.

5 EXPERIMENTAL RESULTS

We conduct experiments using real data to verify the performance of the proposed algorithms. We compare with existing tensor ring completion algorithms, including PTRC [13], TRNN [19] and TRNN-L1 [20]. We also compare with robust tensor completion algorithms under other tensor rank models, including the Tucker rank-based algorithms SNN-L1 [4] and SNN-WST [5], and the tubal rank-based algorithm TNN-L1 [28]. For the proposed methods, we use the three loss functions, Welsch, Cauchy and Huber, designated with a suffix "-W", "-C", and "-H", respectively, appended to the name of the algorithm.

The completion performance is evaluated using the peak signal-to-noise ratio (PSNR) and the structural similarity index measure (SSIM). For each experiment, the average PSNR and SSIM values are obtained over 20 Monte Carlo runs with different missing entries and noise realizations. The rank \hat{r}_k is set to $\lceil qL_k \rceil$ and $2\lceil qL_k \rceil$ for HQTRC-MF and HQTRC-TS, respectively, where L_k denotes the smaller dimension of matrix $\mathbf{X}_{(k,d)}$. The parameter q will be specified later in the experiment. For HQTRC-MF, we set $\beta_k = 1/N$ for all k and $\lambda = 1$. For HQTRC-TS, we set $\mu = 10^{-4}$, $\lambda = 2\mu N$, and $\alpha = 1.1$. For adaptive selection of the parameter c , the parameters in (11) are set to $\eta = 4$, $c_{min} = 0.15$ for the Welsch and Cauchy function, and $\eta = 2$, $c_{min} = 0.05$ for the Huber function. The parameters d and ϵ are set to $\lceil N/2 \rceil$ and 10^{-3} for both proposed algorithms. For the other algorithms, the parameters are adjusted so as to achieve the best performance. Further, the parameters are fixed during each simulation.

5.1 Color image inpainting

In this section, we verify the robust completion performance on an image inpainting task, along with comparison with other existing tensor ring completion algorithms. Image

inpainting takes advantage of the fact most natural images can be approximated with their low-rank components, such that filling missing parts of an incomplete image can be regarded as a tensor completion problem.

Four test images with size $320 \times 480 \times 3$ are selected from the Berkeley Segmentation Dataset [33]. For each image, the pixel value is first normalized to $[0, 1]$. Then, $p n_1 n_2 n_3$ pixels are selected uniformly at random and removed for some fraction p , and $\gamma \times 100\%$ of the observed pixels are perturbed with i.i.d. additive noise generated from a Gaussian distribution with variance σ_o^2 . The image inpainting task is then formulated as a $320 \times 480 \times 3$ robust tensor completion problem with missing data level p and noise level γ . Since the completion performance is known to vary with the tensor order N , we evaluate the performance on different tensor orders. Specifically, the 3-order tensor of size $320 \times 480 \times 3$ is reshaped to a 5-order tensor of size $16 \times 20 \times 20 \times 24 \times 3$ and a 9-order tensor of size $4 \times 4 \times 4 \times 5 \times 4 \times 4 \times 5 \times 6 \times 3$.

First, we present completion results for four test images using different tensor orders. The simulation parameters are set to $p = 50\%$, $\gamma = 20\%$ and $\sigma_o^2 = 0.25$. Table 1 shows the completion performance with different sizes of tensors for four test images. One can observe that the proposed HQTRC-TS achieves the overall best performance (i.e., high PSNR and low SSIM) with tensor order 9. Moreover, the proposed methods with different M-estimator functions achieve comparable good performance for tensor order 5 and 9. Fig. 2 shows an example of the recovered frames from the four images with tensor order $N = 9$. It can be seen that only the proposed M-estimator-based completion methods successfully recover the image, while the other algorithms fail to recognize and remove noisy pixels.

Second, to investigate performance under different noise levels and percentages of missing data, we obtain the phase transition in the $\gamma - p$ plane using the flower image. The variance is set to $\sigma_o^2 = 0.25$, and q for rank estimation is set to $0.2\sqrt{1-p}$. For each simulation, both the noise level γ and the missing data level p are increased from 0 to 0.9, and the SSIM is obtained for different algorithms. The phase transitions for different order N and different algorithms are shown in Fig.3, and an example of the recovered images is shown in Fig.4. The results demonstrate the superior performance of the proposed methods compared with existing tensor-ring-based completion algorithms in different noisy environments. It can be seen that the proposed methods with both truncated SVD and matrix factorization yield clearer and smoother texture using 9-order tensor.

5.2 Video completion

In this part, we compare the performance of the proposed method with existing robust tensor completion algorithms in video completion task. The completion performance is evaluated using color video sequences from the YUV dataset [34]. For each video, a sequence of 60 frames is selected, and each frame is resized to 144×180 to obtain a tensor of size $144 \times 180 \times 3 \times 60$. Similar to the previous section, a tensor with noisy and missing entries is generated by removing 70% of the pixels then adding i.i.d. Gaussian noise with variance 0.25 to $\gamma \times 100\%$ of the observed

TABLE 1
Completion performance (PSNR and SSIM) comparison for different algorithms on four images.

Image	N	Metric	TRMF	TRNN	TRNN-L1	HQTRC-MF -W	HQTRC-MF -C	HQTRC-MF -H	HQTRC-TS -W	HQTRC-TS -C	HQTRC-TS -H
House	3	PSNR	14.76	14.77	22.26	18.03	18.62	18.73	19.12	19.54	19.81
		SSIM	0.2737	0.2631	0.7029	0.6097	0.6129	0.5923	0.6528	0.6585	0.6582
	5	PSNR	15.21	15.00	16.84	23.20	23.25	23.05	25.79	25.59	25.66
		SSIM	0.2985	0.2745	0.3384	0.7452	0.7393	0.7396	0.8119	0.8007	0.8104
	9	PSNR	15.32	15.12	15.23	24.96	24.91	24.84	26.22	26.04	26.12
		SSIM	0.3071	0.2815	0.2837	0.8051	0.7951	0.8006	0.8376	0.8268	0.8376
Church	3	PSNR	14.96	14.91	23.57	18.87	19.56	19.20	18.70	20.09	19.74
		SSIM	0.3721	0.3604	0.8921	0.7804	0.7791	0.7787	0.8280	0.8403	0.8387
	5	PSNR	15.36	15.13	17.28	24.33	24.27	23.79	27.16	26.82	26.86
		SSIM	0.4058	0.3732	0.4678	0.8855	0.8807	0.8815	0.9137	0.9064	0.9121
	9	PSNR	15.46	15.25	15.36	27.06	26.91	26.86	27.64	27.36	27.58
		SSIM	0.4161	0.3813	0.3828	0.9252	0.9194	0.9231	0.9235	0.9171	0.9248
Flower	3	PSNR	14.86	14.89	23.89	18.10	18.98	19.33	18.70	20.09	19.74
		SSIM	0.4592	0.4537	0.8984	0.7506	0.7578	0.7357	0.8280	0.8403	0.8387
	5	PSNR	15.32	15.10	17.23	23.87	24.13	23.82	27.16	26.82	26.86
		SSIM	0.4803	0.4665	0.5417	0.8680	0.8612	0.8679	0.9137	0.9064	0.9121
	9	PSNR	15.41	15.22	15.32	26.65	26.52	26.57	27.64	27.36	27.58
		SSIM	0.4839	0.4729	0.4751	0.9099	0.9005	0.9070	0.9235	0.9171	0.9248
Bridge	3	PSNR	15.44	15.24	26.30	25.24	25.11	25.15	25.80	25.78	25.66
		SSIM	0.3286	0.3071	0.8349	0.7760	0.7638	0.7711	0.8193	0.8206	0.8231
	5	PSNR	15.44	15.46	18.29	26.73	26.53	26.72	27.79	27.44	27.84
		SSIM	0.3334	0.3141	0.4142	0.8222	0.8103	0.8193	0.8580	0.8447	0.8585
	9	PSNR	15.52	15.52	15.65	27.71	27.47	27.71	27.87	27.56	27.99
		SSIM	0.3380	0.3181	0.3202	0.8456	0.8344	0.8435	0.8632	0.8532	0.8690



Fig. 2. Example of the recovered video frames using different algorithms ($N = 9$).

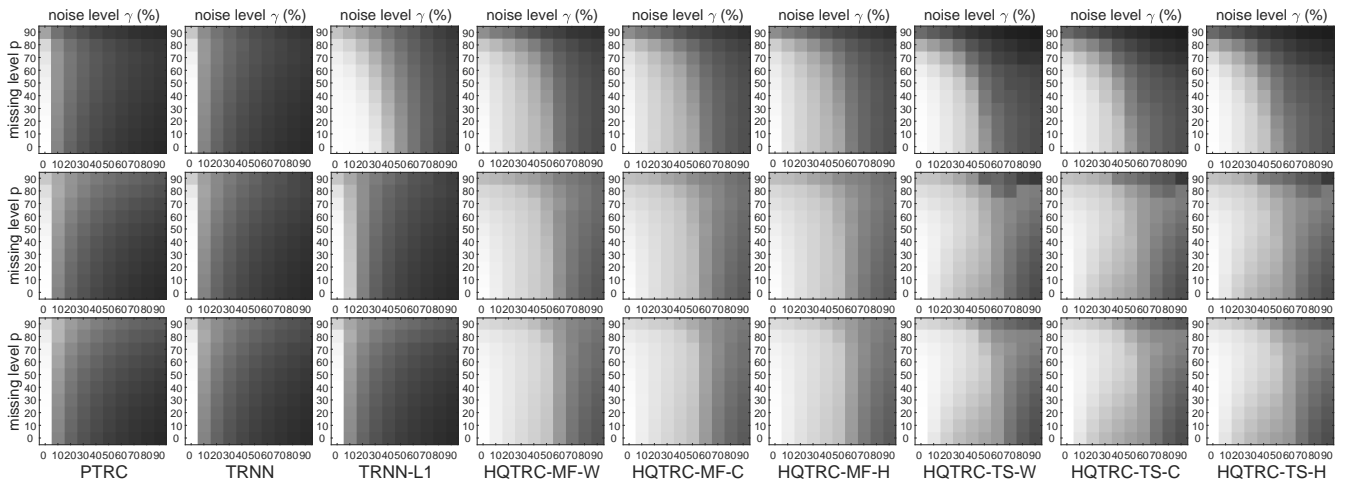


Fig. 3. Phase transition images of different noise level γ and missing level p (From top to bottom: $N = 3$, $N = 5$, $N = 9$).

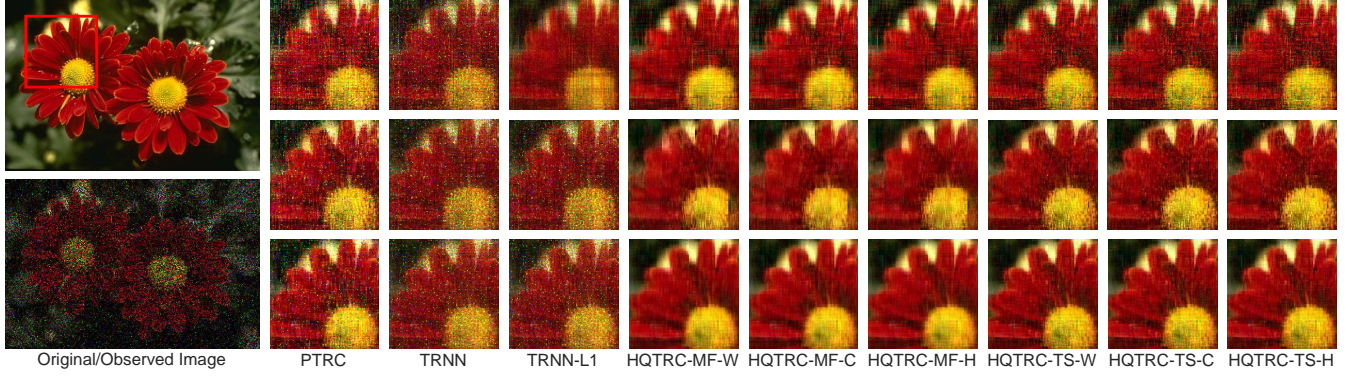


Fig. 4. Example of the recovered image using different algorithms ($\gamma = 30\%$, $p = 60\%$, from top to bottom: $N = 3$, $N = 5$, $N = 9$).

TABLE 2
Completion performance (PSNR and SSIM) comparison for different algorithms on four video sequences.

Video	γ	Metric	TRNN-L1	SNN-WST	SNN-L1	TNN-L1	HQTRC-MF (N=5)	HQTRC-MF (N=12)	HQTRC-TS (N=5)	HQTRC-TS (N=12)
Flower	10%	PSNR	21.48	20.64	19.86	22.55	21.85	22.39	23.12	23.44
		SSIM	0.6556	0.7410	0.5671	0.7628	0.7662	0.8104	<u>0.8289</u>	0.8661
	30%	PSNR	17.62	19.50	16.00	21.76	21.15	21.76	<u>22.25</u>	22.36
		SSIM	0.3759	0.6252	0.3157	<u>0.7373</u>	0.6397	0.7291	<u>0.7149</u>	0.8266
	50%	PSNR	14.53	16.57	13.55	20.63	19.79	20.61	20.44	20.36
		SSIM	0.2605	0.3421	0.2342	<u>0.5965</u>	0.4815	<u>0.5778</u>	0.5155	0.7008
Stefan	10%	PSNR	21.51	20.16	18.99	20.75	21.13	21.72	22.43	23.05
		SSIM	0.7589	0.7078	0.6449	0.6521	0.7391	0.7678	<u>0.8049</u>	0.8351
	30%	PSNR	17.43	19.10	15.87	20.11	20.52	21.16	<u>21.59</u>	22.15
		SSIM	0.4788	0.6530	0.3920	0.6314	0.6846	0.7374	<u>0.7465</u>	0.7978
	50%	PSNR	14.43	16.30	13.44	19.05	19.28	20.03	<u>19.63</u>	20.00
		SSIM	0.2925	0.4490	0.2557	0.5714	0.5916	<u>0.6716</u>	0.5890	0.7085
Bus	10%	PSNR	21.47	20.15	18.85	21.70	20.81	<u>21.88</u>	21.74	23.35
		SSIM	0.6586	0.5682	0.4745	0.5194	0.5835	<u>0.6550</u>	0.6668	0.7258
	30%	PSNR	17.41	18.92	15.29	20.89	20.22	<u>21.35</u>	20.96	22.56
		SSIM	0.3523	0.4708	0.2515	0.4646	0.4983	<u>0.5970</u>	0.5691	0.6805
	50%	PSNR	14.32	16.02	13.01	19.53	18.89	<u>20.32</u>	19.17	20.41
		SSIM	0.2139	0.2691	0.1605	0.3655	0.3807	<u>0.5027</u>	0.3940	0.5369
Coastguard	10%	PSNR	26.21	23.93	22.67	27.32	26.48	27.01	28.93	29.27
		SSIM	0.8464	0.7349	0.6575	0.7522	0.8258	0.8242	0.8962	<u>0.8860</u>
	30%	PSNR	20.14	23.02	17.26	26.09	25.10	25.78	26.80	27.27
		SSIM	0.4547	0.6617	0.3044	0.7183	0.7356	0.7646	<u>0.8073</u>	0.8300
	50%	PSNR	15.50	18.94	14.25	24.23	23.35	24.21	<u>24.02</u>	24.56
		SSIM	0.2314	0.3965	0.1827	<u>0.6311</u>	0.6437	<u>0.6848</u>	0.6558	0.7338

pixels. The observed tensor is reshaped to a 5-order tensor of size $144 \times 180 \times 3 \times 6 \times 10$ and a 12-order of size $3 \times 3 \times 4 \times 4 \times 3 \times 3 \times 4 \times 5 \times 3 \times 3 \times 4 \times 5$. Since Section 5.1 shows similar performance of the algorithms using the three loss functions, in this experiment we only select the Cauchy loss function for comparison and the suffix "-C" is omitted. The parameter q for rank estimation is set to $0.1\sqrt{1-p}$. For SNN-L1, SNN-WST and TNN-L1 we use the reshaped tensor with size $144 \times 180 \times 180$ to obtain better results.

Table 2 shows the average PSNR and SSIM for different algorithms on four video sequences with different noise level γ . The SSIM value of a video is computed as the average value of SSIM between the recovered and the original frames. One can observe that the proposed HQTRC-TS with $N = 12$ achieves the best overall performance, and HQTRC-MF comes second. Fig.6 shows an example of the recovered frames from the four sequences with $\gamma = 30\%$. It can be seen that TNN-L1 and the two methods proposed successfully mitigate the effect of large outliers and recover all four

frames. Further, the colors in the frames recovered using the proposed methods with $N = 12$ are more accurately recovered compared with the other algorithms.

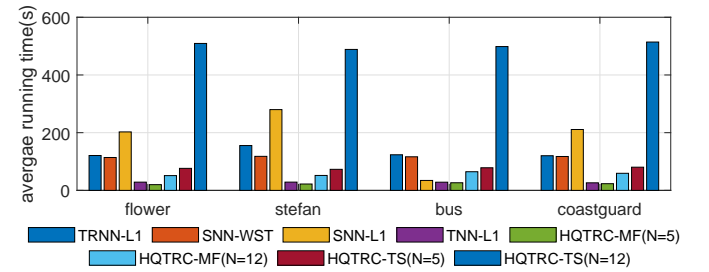


Fig. 5. Average running times for different algorithms on four video sequences ($\gamma = 30\%$).

We also compare the computational efficiency of the algorithms. The average running time for different algorithms is shown in Fig.5. Although HQTRC-TS with $N = 12$ achieves the best performance, it incurs longer running time

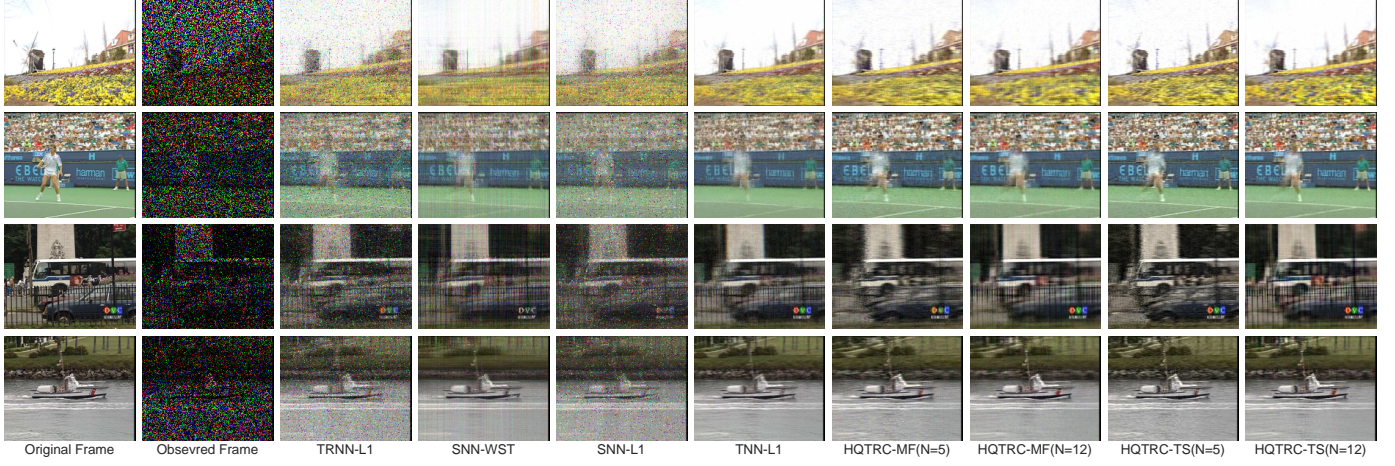


Fig. 6. Example of the recovered video frames using different algorithms ($\gamma = 30\%$).

than the other algorithms due to the high computational cost of the SVD computation (even when truncated SVD is faster than full SVD). By contrast, HQTRC-MF has smaller running time due to the use of efficient matrix factorization. While this highlights a tradeoff between accuracy and computational efficiency, HQTRC-MF incurs a much lower running time than HQTRC-TS with a relatively small loss in accuracy.

5.3 Hyper-spectral image completion and denoising

Hyper-spectral images consist of several images in different bands generated with fine spectral resolution. Many such images are naturally contaminated with noise, thus we aim to verify the robustness of the proposed approach with real noise. We use the Indian Pines dataset [35], which consists of 145×145 pixels and 220 spectral bands. We resize the image to 144×180 , yielding a tensor of size $144 \times 180 \times 220$. To simultaneously verify the completion and denoising performance, 20% of the entries are randomly selected and used to reconstruct the missing entries of the tensor as well as denoise the entire tensor. For tensor ring-based algorithms, the tensor is reshaped to a 11-order tensor of size $3 \times 3 \times 4 \times 4 \times 3 \times 3 \times 4 \times 4 \times 4 \times 5 \times 11$. The algorithm parameters are set to the same as in the previous section. Fig. 7 shows the three recovered images with histogram equalization using different algorithms. For the first image which originally comes with low noise level, all the recovered images have clear, smooth texture with less noise. However, for the last two images which contain high levels of noise, the proposed HQTRC-TS yields a relatively smoother and clearer texture than the other algorithms.

6 CONCLUSION

We proposed a novel robust M-estimation-based tensor ring completion method. The M-estimator is used for the error residuals such that the impact of large outliers can be reduced. A half-quadratic method is leveraged to solve the complex and non-convex problem. Two efficient algorithms using truncated SVD and matrix factorization are developed and their convergence is analyzed. Experimental results verify the superior performance compared with existing tensor completion algorithms in different noisy environments.

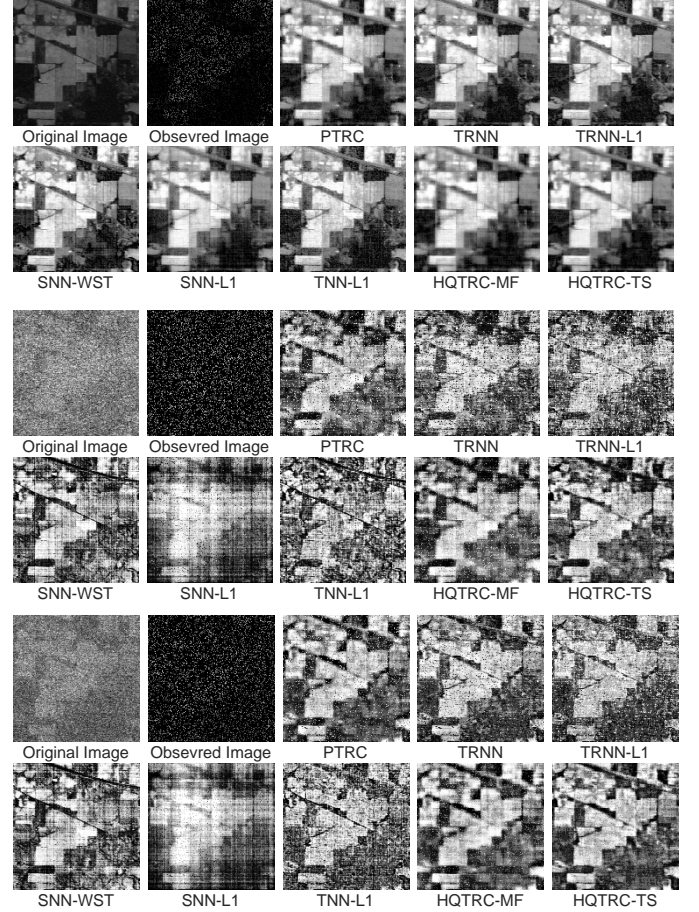


Fig. 7. Recovered hyper-spectral images using different algorithms. From top to bottom: band 210, 105 and 163.

APPENDIX A PROOF OF THEOREM 1

First, we obtain the relation between \mathcal{X}^t and \mathcal{X}^{t+1} . Since $\{\mathcal{G}^{(k),t}\}$ converges to \mathcal{C} , we conclude from (21) that $\{\mathcal{Z}^{(k),t} - \mathcal{X}^t\}$ converges to 0 for all $k = 1, \dots, N$. Thus, for $t \rightarrow \infty$, from (18) we have

$$\lim_{t \rightarrow \infty} \mathbf{X}_{(k,d)}^{t+1} = \lim_{t \rightarrow \infty} \Pi_{\hat{r}_k}(\mathbf{X}_{(k,d)}^t - \mu^{-1} \mathbf{C}_{(k,d)}) \quad (\text{S.1})$$

We will need the following lemma, whose proof is given in Appendix B.

Lemma 1. *If matrices $\mathbf{A}, \mathbf{B}, \mathbf{C} \in \mathbb{R}^{m \times n}$ are such that*

$$\mathbf{A} = \Pi_r(\mathbf{B} - \mathbf{C}),$$

where $\Pi_r(\cdot)$ is the truncated SVD operator with rank r , then at least one of the following results must hold:

- 1) $\|\mathbf{A}\|_F^2 < \|\mathbf{B}\|_F^2$.
- 2) $\|\mathbf{B} - \mathbf{A}\|_F^2 \leq 2\|\mathbf{C}\|_F^2$.

According to Lemma 1, we conclude that at least one of the following results is satisfied:

- 1) $\lim_{t \rightarrow \infty} \|\mathcal{X}^{t+1}\|_F^2 < \lim_{t \rightarrow \infty} \|\mathcal{X}^t\|_F^2$,
- 2) $\lim_{t \rightarrow \infty} \|\mathcal{X}^{t+1} - \mathcal{X}^t\|_F^2 \leq 2\mu^{-2}\|\mathcal{C}\|_F^2$.

If result 1 holds, then we readily have convergence. Therefore, in the following, we analyze the case in which result 2 holds.

By replacing $\mathcal{Z}^{(k),t+1}$ and $\mathcal{G}^{(k),t+1}$ in (20) with \mathcal{X}^{t+1} and \mathcal{C} , respectively, we obtain

$$\begin{aligned} \lim_{t \rightarrow \infty} \mathcal{Q}^{t+1} &= \lim_{t \rightarrow \infty} \mathcal{X}^{t+1} + \mu^{-1}\mathcal{C} \\ \lim_{t \rightarrow \infty} \mathcal{X}^{t+1} &= \lim_{t \rightarrow \infty} \mathcal{Q}^{t+1} + \frac{\lambda \mathcal{W}^{t+1}}{\lambda \mathcal{W}^{t+1} + \mu N} \circ \mathcal{P} \circ (\mathcal{M} - \mathcal{Q}^{t+1}) \end{aligned} \quad (\text{S.2})$$

We can easily derive that $\mathcal{C}_{i_1 \dots i_N} = 0$ for $(i_1 \dots i_N) \notin \Omega$. Next, we show that for $(i_1 \dots i_N) \in \Omega$, $\lim_{c \rightarrow 0} \mathcal{C}_{i_1 \dots i_N} = 0$. Here, we use the Welsch function as an example. By applying the Welsch function to the second term on the RHS of (20), we have for all $(i_1 \dots i_N) \in \Omega$

$$\begin{aligned} \lim_{t \rightarrow \infty} \mathcal{W}_{i_1 \dots i_N}^{t+1} (\mathcal{M}_{i_1 \dots i_N} - \mathcal{Q}_{i_1 \dots i_N}^{t+1}) \\ = \lim_{t \rightarrow \infty} \exp \left(-\frac{(\mathcal{M}_{i_1 \dots i_N} - \mathcal{X}_{i_1 \dots i_N}^t)^2}{2(c^{t+1})^2} \right) (\mathcal{M}_{i_1 \dots i_N} - \mathcal{X}_{i_1 \dots i_N}^{t+1} \\ - \mu^{-1}\mathcal{C}_{i_1 \dots i_N}). \end{aligned} \quad (\text{S.3})$$

Since $\lim_{t \rightarrow \infty} \|\mathcal{X}^{t+1} - \mathcal{X}^t\|_F^2 \leq 2\mu^{-2}\|\mathcal{C}\|_F^2$, we get that $\lim_{t \rightarrow \infty} |\mathcal{X}_{i_1 \dots i_N}^{t+1} - \mathcal{X}_{i_1 \dots i_N}^t| \leq 2\mu^{-2}\|\mathcal{C}\|_F^2$, thus we have

$$a \leq \lim_{t \rightarrow \infty} \mathcal{W}_{i_1 \dots i_N}^{t+1} (\mathcal{M}_{i_1 \dots i_N} - \mathcal{Q}_{i_1 \dots i_N}^{t+1}) \leq b \quad (\text{S.4})$$

where

$$\begin{aligned} a &= \lim_{t \rightarrow \infty} \exp \left(-\frac{(\mathcal{E}_{i_1 \dots i_N}^t)^2}{2(c^{t+1})^2} \right) (\mathcal{E}_{i_1 \dots i_N}^t - \mu^{-1}\mathcal{C}_{i_1 \dots i_N} - 2\mu^{-2}\|\mathcal{C}\|_F^2) \\ b &= \lim_{t \rightarrow \infty} \exp \left(-\frac{(\mathcal{E}_{i_1 \dots i_N}^t)^2}{2(c^{t+1})^2} \right) (\mathcal{E}_{i_1 \dots i_N}^t - \mu^{-1}\mathcal{C}_{i_1 \dots i_N} + 2\mu^{-2}\|\mathcal{C}\|_F^2) \end{aligned}$$

where $\mathcal{E}_{i_1 \dots i_N}^t = \mathcal{M}_{i_1 \dots i_N} - \mathcal{X}_{i_1 \dots i_N}^t$. For the Welsch function $f(x) = c^2(1 - \exp(-x^2/(2c^2)))$, $x \in \mathbb{R}$, $f'(x) = x \exp(-x^2/(2c^2)) \in [-ce^{-0.5}, ce^{-0.5}]$, therefore a and b are bounded for any $\mathcal{X}_{i_1 \dots i_N}^t$. It can be also observed that both a and b are 0 when $c \rightarrow 0$ and $\lim_{t \rightarrow \infty} \mathcal{E}_{i_1 \dots i_N}^t \neq 0$, which indicates that $\lim_{t \rightarrow \infty} \mathcal{W}_{i_1 \dots i_N}^{t+1} (\mathcal{M}_{i_1 \dots i_N} - \mathcal{Q}_{i_1 \dots i_N}^{t+1}) = 0$, and using (S.2) one can further obtain $\lim_{c \rightarrow 0} \mathcal{C}_{i_1 \dots i_N} = 0$. For the case where $\lim_{t \rightarrow \infty} \mathcal{E}_{i_1 \dots i_N}^t = 0$, we have that $\lim_{t \rightarrow \infty} \mathcal{X}_{i_1 \dots i_N}^{t+1} = \lim_{t \rightarrow \infty} \mathcal{M}_{i_1 \dots i_N}$, which means $\{\mathcal{X}_{i_1 \dots i_N}^t\}$ converges and thus $\mathcal{C}_{i_1 \dots i_N} = 0$. Therefore, we conclude that $\lim_{c \rightarrow 0} \mathcal{C}_{i_1 \dots i_N} = 0$ for all entries $(i_1 \dots i_N)$, i.e., $\lim_{c \rightarrow 0} \mathcal{C} = 0$.

The key point of the above analysis is the boundedness of $f'(x)$. Since $f'(x)$ is also bounded for the Cauchy and Huber functions, a similar result can be derived.

Therefore, under result 2, $\lim_{c \rightarrow 0} \mathcal{C} = 0$, which implies that $\lim_{c \rightarrow 0} \lim_{t \rightarrow \infty} \mathcal{X}^{t+1} = \lim_{c \rightarrow 0} \lim_{t \rightarrow \infty} \mathcal{X}^t$. Combining both results 1 and 2, we have that the sequence $\{\mathcal{X}^t\}$ converges as $c \rightarrow 0$.

APPENDIX B

PROOF OF LEMMA 1

Without loss of generality, we assume $m \leq n$. Then, we define $\sigma_i(\mathbf{X})$ as the i -th eigenvalue of matrix \mathbf{X} , where $\sigma_m(\mathbf{X}) \geq \sigma_{m-1}(\mathbf{X}) \geq \dots \geq \sigma_1(\mathbf{X}) \geq 0$. Using the relation between the eigenvalues of a matrix and its Frobenius norm, we get

$$\begin{aligned} \|\mathbf{B} - \mathbf{C}\|_F^2 &= \sum_{i=1}^m \sigma_i^2(\mathbf{B} - \mathbf{C}) \\ &= \sum_{i=1}^{r-1} \sigma_i^2(\mathbf{B} - \mathbf{C}) + \sum_{i=r}^m \sigma_i^2(\mathbf{B} - \mathbf{C}) \quad (\text{S.5}) \\ &= \|(\mathbf{B} - \mathbf{C}) - \mathbf{A}\|_F^2 + \|\mathbf{A}\|_F^2 \\ &\geq \|\mathbf{B} - \mathbf{A}\|_F^2 - \|\mathbf{C}\|_F^2 + \|\mathbf{A}\|_F^2 \end{aligned}$$

If $\|\mathbf{B} - \mathbf{A}\|_F^2 \leq \|\mathbf{C}\|_F^2$, result 2 in the Lemma is satisfied. Otherwise, we have $\|\mathbf{B} - \mathbf{A}\|_F^2 - \|\mathbf{C}\|_F^2 = \|\mathbf{B} - \mathbf{A}\|_F^2 - \|\mathbf{C}\|_F^2$. Further, combining the property that $\|\mathbf{B} - \mathbf{C}\|_F^2 \leq \|\mathbf{B}\|_F^2 + \|\mathbf{C}\|_F^2$, we derive from (S.5) that

$$\|\mathbf{B} - \mathbf{A}\|_F^2 \leq \|\mathbf{B}\|_F^2 - \|\mathbf{A}\|_F^2 + 2\|\mathbf{C}\|_F^2. \quad (\text{S.6})$$

If $\|\mathbf{A}\|_F^2 < \|\mathbf{B}\|_F^2$, result 1 is satisfied. Otherwise, we have

$$\|\mathbf{B} - \mathbf{A}\|_F^2 \leq 2\|\mathbf{C}\|_F^2, \quad (\text{S.7})$$

i.e., result 2 holds.

APPENDIX C

PROOF OF CONVERGENCE OF THEOREM 2.2

For simplicity, we define

$$\begin{aligned} J_c(\mathcal{X}, \mathcal{W}, \mathbf{U}_a, \mathbf{V}_a) &= \sum_{k=1}^N \frac{\beta_k}{2} \|\mathbf{U}_k \mathbf{V}_k - \mathbf{X}_{\langle k, d \rangle}\|_F^2 \\ &\quad + \frac{\lambda}{2} \|\sqrt{\mathcal{W}} \circ \mathcal{P} \circ (\mathcal{M} - \mathcal{X})\|_F^2 \\ &\quad + \lambda \Psi_\Omega(\mathcal{W}). \end{aligned} \quad (\text{S.8})$$

Hence,

$$\begin{aligned} J_c(\mathcal{X}^t, \mathcal{W}^t, \mathbf{U}_a^t, \mathbf{V}_a^t) - J_c(\mathcal{X}^t, \mathcal{W}^t, \mathbf{U}_a^{t+1}, \mathbf{V}_a^{t+1}) \\ = \sum_{k=1}^N \frac{\beta_k}{2} \left(\|\mathbf{U}_k^t \mathbf{V}_k^t - \mathbf{X}_{\langle k, d \rangle}^t\|_F^2 - \|\mathbf{U}_k^{t+1} \mathbf{V}_k^{t+1} - \mathbf{X}_{\langle k, d \rangle}^t\|_F^2 \right) \\ = \sum_{k=1}^N \frac{\beta_k}{2} \|\mathbf{U}_k^{t+1} \mathbf{V}_k^{t+1} - \mathbf{U}_k^t \mathbf{V}_k^t\|_F^2 \end{aligned} \quad (\text{S.9})$$

where the last equation follows from Lemma 4.2 in [36]. Further, since \mathcal{W} is the optimal solution to the following optimization problem

$$\mathcal{W}^{t+1} = \arg \min_{\mathcal{W}} \frac{1}{2} \|\sqrt{\mathcal{W}} \circ \mathcal{P} \circ (\mathcal{M} - \mathcal{X}^t)\|_F^2 + \Psi_\Omega(\mathcal{W}) \quad (\text{S.10})$$

and \mathcal{X} is the optimal solution of (23), we have that

$$\begin{aligned} J_{c^{t+1}}(\mathcal{X}^{t+1}, \mathcal{W}^{t+1}, \mathbf{U}_a^{t+1}, \mathbf{V}_a^{t+1}) \\ \leq J_{c^{t+1}}(\mathcal{X}^t, \mathcal{W}^t, \mathbf{U}_a^{t+1}, \mathbf{V}_a^{t+1}). \end{aligned} \quad (\text{S.11})$$

It is not hard to prove that for a fixed argument x , the loss function $f(c)$ satisfies $f'(c) > 0$ for $c > 0$. Thus, given a fixed \mathcal{X} , the function $F_\sigma(\mathcal{X} - \mathcal{M})$ monotonically decreases as c decreases. Therefore, according to (7) and (S.10), and using the assumption $c^{t+1} \leq c^t$, we have that

$$J_{c^{t+1}}(\mathcal{X}^t, \mathcal{W}^t, \mathbf{U}_a^{t+1}, \mathbf{V}_a^{t+1}) \leq J_{c^t}(\mathcal{X}^t, \mathcal{W}^t, \mathbf{U}_a^{t+1}, \mathbf{V}_a^{t+1}) \quad (\text{S.12})$$

Therefore,

$$\begin{aligned} J_{c^t}(\mathcal{X}^t, \mathcal{W}^t, \mathbf{U}_a^t, \mathbf{V}_a^t) - J_{c^{t+1}}(\mathcal{X}^{t+1}, \mathcal{W}^{t+1}, \mathbf{U}_a^{t+1}, \mathbf{V}_a^{t+1}) \\ = J_{c^t}(\mathcal{X}^t, \mathcal{W}^t, \mathbf{U}_a^t, \mathbf{V}_a^t) - J_{c^t}(\mathcal{X}^t, \mathcal{W}^t, \mathbf{U}_a^{t+1}, \mathbf{V}_a^{t+1}) \\ + J_{c^t}(\mathcal{X}^t, \mathcal{W}^t, \mathbf{U}_a^{t+1}, \mathbf{V}_a^{t+1}) \\ - J_{c^{t+1}}(\mathcal{X}^{t+1}, \mathcal{W}^{t+1}, \mathbf{U}_a^{t+1}, \mathbf{V}_a^{t+1}) \\ \geq \sum_{k=1}^N \frac{\beta_k}{2} \|\mathbf{U}_k^{t+1} \mathbf{V}_k^{t+1} - \mathbf{U}_k^t \mathbf{V}_k^t\|_F^2, \end{aligned} \quad (\text{S.13})$$

which implies that $J_{c^t}(\mathcal{X}^t, \mathcal{W}^t, \mathbf{U}_a^t, \mathbf{V}_a^t) \geq J_{c^{t+1}}(\mathcal{X}^{t+1}, \mathcal{W}^{t+1}, \mathbf{U}_a^{t+1}, \mathbf{V}_a^{t+1})$.

By summing over n iterations on both sides of the inequality, we get that

$$\begin{aligned} J_{c^0}(\mathcal{X}^0, \mathcal{W}^0, \mathbf{U}_a^0, \mathbf{V}_a^0) - J_{c^n}(\mathcal{X}^n, \mathcal{W}^n, \mathbf{U}_a^n, \mathbf{V}_a^n) \\ \geq \sum_{t=0}^n \sum_{k=1}^N \frac{\beta_k}{2} \|\mathbf{U}_k^{t+1} \mathbf{V}_k^{t+1} - \mathbf{U}_k^t \mathbf{V}_k^t\|_F^2. \end{aligned} \quad (\text{S.14})$$

Since $\Psi_\Omega(\mathcal{W}) \geq 0$ [26], J is lower bounded by zero. Hence,

$$\lim_{t \rightarrow +\infty} \|\mathbf{U}_k^{t+1} \mathbf{V}_k^{t+1} - \mathbf{U}_k^t \mathbf{V}_k^t\|_F^2 = 0. \quad (\text{S.15})$$

Consequently, the sequences $\{\mathcal{X}^t\}$ and $\{\mathcal{W}^t\}$ converge. Thus, $\{\mathcal{L}^t\}$ in (23) will converge. We can also obtain from (23) that $\mathcal{X}_{i_1 \dots i_N}^{t+1} = \mathcal{L}_{i_1 \dots i_N}^{t+1}$ for $(i_1 \dots i_N) \notin \Omega$. Further, for $(i_1 \dots i_N) \in \Omega$ with $\lim_{t \rightarrow \infty} \mathcal{E}_{i_1 \dots i_N}^t \neq 0$, we have $\lim_{c \rightarrow 0} \lim_{t \rightarrow \infty} \mathcal{W}_{i_1 \dots i_N}^{t+1} = 0$, in which case we will have $\lim_{c \rightarrow 0} \lim_{t \rightarrow \infty} \mathcal{X}_{i_1 \dots i_N}^{t+1} = \lim_{c \rightarrow 0} \lim_{t \rightarrow \infty} \mathcal{L}_{i_1 \dots i_N}^{t+1}$. While for $(i_1 \dots i_N) \in \Omega$ with $\lim_{t \rightarrow \infty} \mathcal{E}_{i_1 \dots i_N}^t = 0$, we have $\lim_{t \rightarrow \infty} \mathcal{X}_{i_1 \dots i_N}^{t+1} = \mathcal{M}_{i_1 \dots i_N}$. Given the above, along with the convergence of $\{\mathcal{L}^{t+1}\}$, we conclude that $\{\mathcal{X}^t\}$ converges.

ACKNOWLEDGMENTS

This work was supported by NSF CAREER Award CCF-1552497 and NSF Award CCF-2106339.

REFERENCES

- [1] Q. Song, H. Ge, J. Caverlee, and X. Hu, "Tensor completion algorithms in big data analytics," *ACM Transactions on Knowledge Discovery from Data (TKDD)*, vol. 13, no. 1, pp. 1–48, 2019.
- [2] L. Karlsson, D. Kressner, and A. Uschmajew, "Parallel algorithms for tensor completion in the CP format," *Parallel Computing*, vol. 57, pp. 222–234, 2016.
- [3] J. Liu, P. Musialski, P. Wonka, and J. Ye, "Tensor completion for estimating missing values in visual data," *IEEE transactions on pattern analysis and machine intelligence*, vol. 35, no. 1, pp. 208–220, 2012.
- [4] D. Goldfarb and Z. Qin, "Robust low-rank tensor recovery: Models and algorithms," *SIAM Journal on Matrix Analysis and Applications*, vol. 35, no. 1, pp. 225–253, 2014.
- [5] Y. Yang, Y. Feng, and J. A. Suykens, "Robust low-rank tensor recovery with regularized redescending M-estimator," *IEEE transactions on neural networks and learning systems*, vol. 27, no. 9, pp. 1933–1946, 2015.
- [6] L. Yang, J. Fang, H. Li, and B. Zeng, "An iterative reweighted method for Tucker decomposition of incomplete tensors," *IEEE Transactions on Signal Processing*, vol. 64, no. 18, pp. 4817–4829, 2016.
- [7] Z. Zhang and S. Aeron, "Exact tensor completion using t-SVD," *IEEE Transactions on Signal Processing*, vol. 65, no. 6, pp. 1511–1526, 2016.
- [8] P. Zhou, C. Lu, Z. Lin, and C. Zhang, "Tensor factorization for low-rank tensor completion," *IEEE Transactions on Image Processing*, vol. 27, no. 3, pp. 1152–1163, 2017.
- [9] X.-Y. Liu, S. Aeron, V. Aggarwal, and X. Wang, "Low-tubal-rank tensor completion using alternating minimization," *IEEE Transactions on Information Theory*, vol. 66, no. 3, pp. 1714–1737, 2019.
- [10] W. Wang, V. Aggarwal, and S. Aeron, "Efficient low rank tensor ring completion," in *Proceedings of the IEEE International Conference on Computer Vision*, 2017, pp. 5697–5705.
- [11] L. Yuan, C. Li, D. Mandic, J. Cao, and Q. Zhao, "Tensor ring decomposition with rank minimization on latent space: An efficient approach for tensor completion," in *Proceedings of the AAAI Conference on Artificial Intelligence*, vol. 33, 2019, pp. 9151–9158.
- [12] H. Huang, Y. Liu, J. Liu, and C. Zhu, "Provable tensor ring completion," *Signal Processing*, vol. 171, p. 107486, 2020.
- [13] J. Yu, G. Zhou, C. Li, Q. Zhao, and S. Xie, "Low tensor-ring rank completion by parallel matrix factorization," *IEEE transactions on neural networks and learning systems*, 2020.
- [14] J. A. Bengua, H. N. Phien, H. D. Tuan, and M. N. Do, "Efficient tensor completion for color image and video recovery: Low-rank tensor train," *IEEE Transactions on Image Processing*, vol. 26, no. 5, pp. 2466–2479, 2017.
- [15] L. Yuan, Q. Zhao, and J. Cao, "High-order tensor completion for data recovery via sparse tensor-train optimization," in *2018 IEEE international conference on acoustics, speech and signal processing (ICASSP)*. IEEE, 2018, pp. 1258–1262.
- [16] L. Yuan, J. Cao, X. Zhao, Q. Wu, and Q. Zhao, "Higher-dimension tensor completion via low-rank tensor ring decomposition," in *2018 Asia-Pacific Signal and Information Processing Association Annual Summit and Conference (APSIPA ASC)*. IEEE, 2018, pp. 1071–1076.
- [17] Q. Zhao, G. Zhou, S. Xie, L. Zhang, and A. Cichocki, "Tensor ring decomposition," *arXiv preprint arXiv:1606.05535*, 2016.
- [18] A. Ahad, Z. Long, C. Zhu, and Y. Liu, "Hierarchical tensor ring completion," *arXiv preprint arXiv:2004.11720*, 2020.
- [19] J. Yu, C. Li, Q. Zhao, and G. Zhao, "Tensor-ring nuclear norm minimization and application for visual: Data completion," in *ICASSP 2019-2019 IEEE International Conference on Acoustics, Speech and Signal Processing (ICASSP)*. IEEE, 2019, pp. 3142–3146.
- [20] H. Huang, Y. Liu, Z. Long, and C. Zhu, "Robust low-rank tensor ring completion," *IEEE Transactions on Computational Imaging*, vol. 6, pp. 1117–1126, 2020.
- [21] D. E. Tyler, "A distribution-free M-estimator of multivariate scatter," *The annals of Statistics*, pp. 234–251, 1987.
- [22] M. Nikolova and M. K. Ng, "Analysis of half-quadratic minimization methods for signal and image recovery," *SIAM Journal on Scientific computing*, vol. 27, no. 3, pp. 937–966, 2005.
- [23] J. E. Dennis Jr and R. E. Welsch, "Techniques for nonlinear least squares and robust regression," *Communications in Statistics-simulation and Computation*, vol. 7, no. 4, pp. 345–359, 1978.
- [24] W. Liu, P. P. Pokharel, and J. C. Principe, "Correntropy: Properties and applications in non-Gaussian signal processing," *IEEE Transactions on Signal Processing*, vol. 55, no. 11, pp. 5286–5298, 2007.
- [25] R. He, B. Hu, X. Yuan, L. Wang et al., *Robust recognition via information theoretic learning*. Springer, 2014.
- [26] P. Charbonnier, L. Blanc-Féraud, G. Aubert, and M. Barlaud, "Deterministic edge-preserving regularization in computed imaging," *IEEE Transactions on image processing*, vol. 6, no. 2, pp. 298–311, 1997.
- [27] C. Eckart and G. Young, "The approximation of one matrix by another of lower rank," *Psychometrika*, vol. 1, no. 3, pp. 211–218, 1936.

- [28] Q. Jiang and M. Ng, "Robust low-tubal-rank tensor completion via convex optimization." in *IJCAI*, 2019, pp. 2649–2655.
- [29] S. Boyd, N. Parikh, and E. Chu, *Distributed optimization and statistical learning via the alternating direction method of multipliers*. Now Publishers Inc, 2011.
- [30] B. Jiang, S. Ma, and S. Zhang, "Alternating direction method of multipliers for real and complex polynomial optimization models," *Optimization*, vol. 63, no. 6, pp. 883–898, 2014.
- [31] S. Magnússon, P. C. Weeraddana, M. G. Rabbat, and C. Fischione, "On the convergence of alternating direction lagrangian methods for nonconvex structured optimization problems," *IEEE Transactions on Control of Network Systems*, vol. 3, no. 3, pp. 296–309, 2015.
- [32] Y. Zhang, "Restricted low-rank approximation via admm," *arXiv preprint arXiv:1512.01748*, 2015.
- [33] D. Martin, C. Fowlkes, D. Tal, and J. Malik, "A database of human segmented natural images and its application to evaluating segmentation algorithms and measuring ecological statistics," in *Proc. 8th Int'l Conf. Computer Vision*, vol. 2, July 2001, pp. 416–423.
- [34] "YUV Video Sequences," <http://trace.eas.asu.edu/yuv/>.
- [35] M. F. Baumgardner, L. L. Biehl, and D. A. Landgrebe, "220 band aviris hyperspectral image data set: June 12, 1992 Indian pine test site 3," Sep 2015. [Online]. Available: <https://purrr.purdue.edu/publications/1947/1>
- [36] Y. Xu, R. Hao, W. Yin, and Z. Su, "Parallel matrix factorization for low-rank tensor completion," *Inverse Problems and Imaging*, vol. 9, no. 2, pp. 601–624, 2015.